available at www.sciencedirect.com

www.elsevier.com/locate/matchar

Microstructure and nanohardness distribution in a polycrystalline Zn deformed by high strain rate impact

G. Dirras[a,*], A. Ouarem[a], H. Couque[b], J. Gubicza[c], P. Szommer[c], O. Brinza[a]

[a] LSPM, CNRS, UPR 3407, Université Paris 13, 99 avenue Jean Baptiste Clément, 93430 Villetaeuse, France
[b] Nexter-Munitions, 7 route de Guerry, 18023 Bourges Cedex, France
[c] Department of Materials Physics, Eötvös Loránd University, Budapest, P.O.B. 32, H-1518, Hungary

ARTICLE DATA

Article history:
Received 14 January 2011
Received in revised form
4 March 2011
Accepted 8 March 2011

Keywords:
Electron backscatter diffraction
High strain rate
Recovery
Dislocation
Nanohardness

ABSTRACT

Polycrystalline Zn with an average grain size of about 300 μm was deformed by direct impact Hopkinson pressure bar at a velocity of 29 m/s. An inhomogeneous grain structure was found consisting of a center region having large average grain size of 20 μm surrounded by a fine-grained rim with an average grain size of 6 μm. Transmission electron microscopy investigations showed a significant dislocation density in the large-grained area while in the fine-grained rim the dislocation density was negligible. Most probably, the higher strain yielded recrystallization in the outer ring while in the center only recovery occurred. The hardening effect of dislocations overwhelms the smaller grain size strengthening in the center part resulting in higher nanohardness in this region than in the outer ring.

1. Introduction

The high strain rate behavior of materials is increasingly important in many applications from microelectronics to ballistics. Therefore, various studies have been reported on the deformation behavior and microstructural evolution under high strain rate loading conditions [1–5]. It was shown that at a critical strain rate a transition of the controlling deformation mechanism from thermally activated deformation to viscous phonon drag occurred [6]. Later, Zerilli and Armstrong [7] suggested that this behavior could be more accurately interpreted as an increase in dislocation and twin formation rates.

Hopkinson pressure bar (split-Hopkinson and direct impact Hopkinson pressure bars) and Kolsky bar techniques are among the means that are extensively used to characterize the mechanical behavior of face centered cubic (*fcc*) [8,9] body centered cubic (*bcc*) [10,11] and hexagonal close packed (*hcp*) metallic materials [12–14] under high strain rate impact loading. In most cases, one of the striking features of the impact test is the occurrence of localized deformation in the form of adiabatic shear bands [15,16]. The structure within the bands usually consists of recrystallized submicron-sized grains as a consequence of intense strain localization and temperature rise during straining [17], whose combination supposedly triggers recovery and/or recrystallization phenomena. Therefore, high strain rate loading techniques have been considered by some authors as a way to refine grains in metals and alloys [18–21]. It has been shown that the grain refinement in *fcc* metals such as Al [21] and Ni [9] during impact loading was accompanied by changes in crystallographic texture.

The present work applies direct impact Hopkinson pressure bar technique to study the microstructural changes during high strain rate impact test in high purity polycrystalline Zn. The evolution of the microstructure due to the impact loading is discussed in relation with the local mechanical behavior measured by nanoindentation.

* *Corresponding author*. Tel.: +33 1 49 40 34 88; fax: +33 1 49 40 39 38.
E-mail address: dirras@univ-paris13.fr (G. Dirras).

1044-5803/$ – see front matter © 2011 Elsevier Inc. All rights reserved.
doi:10.1016/j.matchar.2011.03.002

2. Experimental Procedure

High purity polycrystalline Zn, whose chemical composition is given in Table 1 was supplied by Vieille Montagne Angleur (Umicore), Belgium, in the form of bar specimens having 100 mm in height and 6 mm in diameter. Cylindrical specimens of about 6 mm in diameter and 3.3 mm in height were prepared by electric discharge machining. Dynamic compression tests were performed by a direct impact Hopkinson pressure bar (DIHPB) system at room temperature (RT) and at a velocity of 29 m/s. Two samples were tested under the same conditions and they showed identical microstructural characteristics. The set-up of the DIHPB device is depicted in Fig. 1. Further details can be found in our previous reports [9,22].

The microstructures before and after impact test were investigated by electron backscattering diffraction (EBSD) technique using a Zeiss Supra 40VP FEG scanning electron microscope (SEM). The EBSD scans covered regions of approximately 1300 μm × 1300 μm using a step size between neighboring measurement positions of 1 μm. Samples for EBSD investigations were prepared by mechanical grinding up to 4000 grit SiC papers and a finish step using OP-S suspension from Struers™. The total duration of the polishing process was about 20 min. The average grain size, the fraction of low angle grain boundaries (LAGBs) and high angle grain boundaries (HAGBs) were extracted from the EBSD scans using an orientation imaging software OIM version 4 from TexSem Laboratories. The EBSD studies were complemented by TEM investigations using a JEOL-2010 electron microscope at an operating voltage of 200 kV. Specimens for TEM investigations were first thinned mechanically and dimpled to about 60 μm. Final thinning was carried out in a Gatan Precision Ion Polishing System (PIPS). The local mechanical behavior was studied by nanohardness measurements using an UMIS nanoindentation device with a Berkovich indenter and applying a maximum load of 5 mN. The indentation rate was 0.15 mN/s. Nanoindentation experiments were performed at different locations of the impacted surface. In each location 400 indentations were carried out arranging the indents in a 20 × 20 matrix. The distance between the neighbouring indents was 20 μm. The mean hardness at each location was calculated by averaging the 400 hardness values determined as:

$$H = \frac{P_m}{24.5h_m^2}, \quad (1)$$

where P_m is the maximum load (5 mN) and h_m is the maximum penetration depth during indentation.

Table 1 – Chemical composition of the Zn sample (data given by Vieille Montagne Angleur, Belgium).

Zn	Pb	Cu	Cd	Fe
base	0.00005%	0.0%	0.00002%	0.00003%

3. Results and Discussion

3.1. Microstructure Characterization

3.1.1. EBSD Investigations

Fig. 2 illustrates the microstructure of the initial sample before high strain rate impact test. The grains are equiaxed having an average grain size of about 300 μm. In Fig. 2a LAGBs are observed inside the grains and are represented as red lines (angle of misorientation ≤ 5°) and green lines (angle of misorientation between 5° and 15°). The total volume fraction of LAGBs is about 15%. Fig. 2b indicates that the majority of the grains have [0001] crystallographic direction normal to the disc surface, corresponding to a strong [0001] texture as illustrated by the color code in the associated standard stereographic projection triangle.

After the direct impact with a striker velocity of 29 m/s, the final diameter of the sample was increased to about 18.50 mm and the thickness of the disc was reduced to 0.07 mm (h), which corresponds to an engineering axial strain, $\varepsilon_{eng} = (h - h_0)/h_0$ of about −0.98 (h_0 is the initial height of the sample). Assuming that an uniaxial state of stress prevails up to the engineering strain of −0.4, the true stress and true strain rate as a function of true strain were calculated from the load and displacement data taken during impact test. These quantities are plotted in Fig. 3 up to the absolute value of true strain of 0.5 that corresponds to the engineering strain of −0.4. It can be seen in Fig. 3 that in the beginning of plastic deformation the strain rate was ~9×10^3 s^{-1} which increased up to 1.5×10^4 s^{-1} at a true strain of −0.5. At the end of the loading, the strain rate (not shown in Fig. 3) is of the order of 10^5 s^{-1}. This value of strain rate falls into the viscous deformation regime where phonon drag has an important effect on dislocation motion [6]. It should be noted that a precise evaluation of the strain rate history for strain exceeding −0.5 will require to conduct a numerical simulation of the experiment to take into account the evolution of the uniaxial stress state to a multi-axial one. This will be a topic of a further work.

Fig. 4 illustrates the microstructure obtained after impact test. The comparison with the initial state revealed a significant evolution of the grain structure due to deformation. Indeed, a gradient of the grain size is observed on the impacted surface. The center of the sample having a diameter of about 4 mm consists of equiaxed coarse grains with an average grain size of about 20 μm, that is 15 times smaller than in the initial state. This central zone is surrounded by an outer ring consisting of even smaller grains whose average size is about 6 μm, that is 50 times smaller than in the initial state. The frontier between these two areas is not sharp. Indeed, islands of coarser grains like those formed in the center of the sample, are immersed in the zone having small grains, and conversely. Some of the isolated small islands are indicated by squares in Fig. 4. It is also worth to note that the distribution of LAGBs is not the same within the two types of microstructure. The central zone with coarser grains exhibits mostly LAGBs with misorientation angle ≤ 5° (red line or red etch pits), while the fine-grained area is mostly populated by LAGBs with relatively high misorientation close to 15° (green lines). The total fraction of LAGBs extrated from Fig. 4 was about 22% (16%

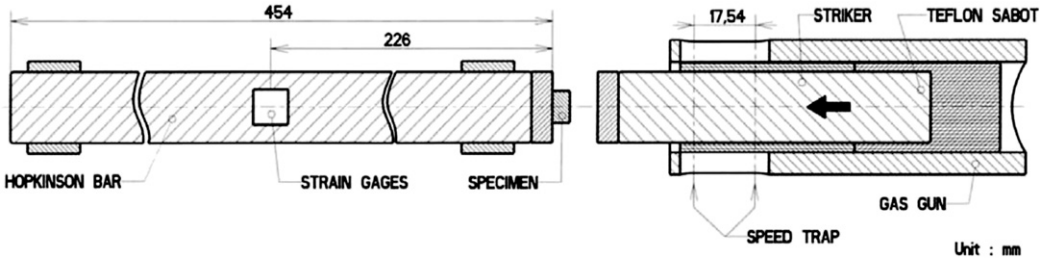

Fig. 1 – A schematic drawing of the direct impact Hopkinson pressure bar system [22].

for LAGBs with a misorientation angle≤5°). The black clusters which are mostly seen in the vicinity of grain boundaries or at triple junctions in Fig. 4 correspond to non indexed areas, probably due to the presence of grains with the size lower than the EBSD step size.

It is noted that the plastic deformation in hexagonal close-packed metals occurs by twinning and/or dislocation slip. In this context, the ratio c/a is a very important parameter. In the case of Zn with $c/a=1.856$ (larger than the ideal value=1.63), mechanical twinning can be activated mainly under compression. For example, Li et al. [23] investigated the fundamental plastic deformation and damage mechanisms in pure Zn under compression and cyclic compression–compression loadings. The main deformation and damage mechanisms

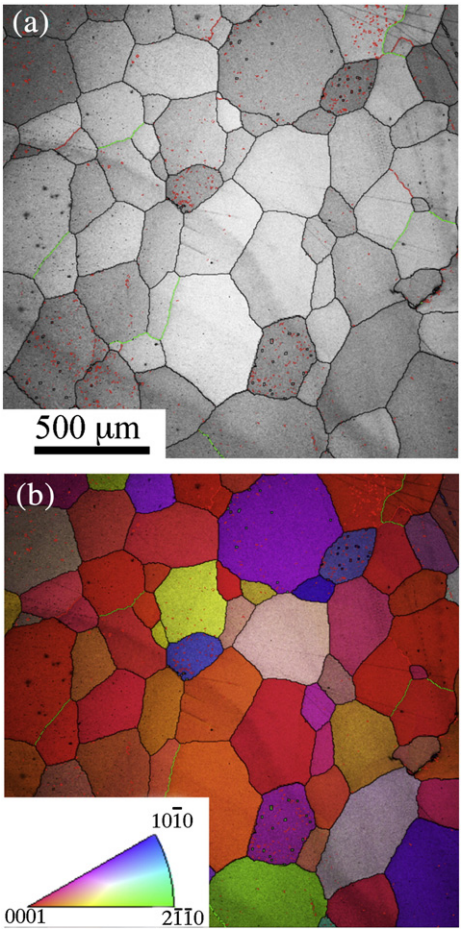

Fig. 2 – (a): EBSD boundary map of the initial microstructure that consists mainly of equiaxed grains bounded by HAGBs. The red and green lines correspond to LAGBs (see the text for more details); (b): EBSD inverse pole figure showing the orientation of grains on the surface of the initial sample. The majority of the grains possess a [0001] axis perpendicular to the surface of the sample.

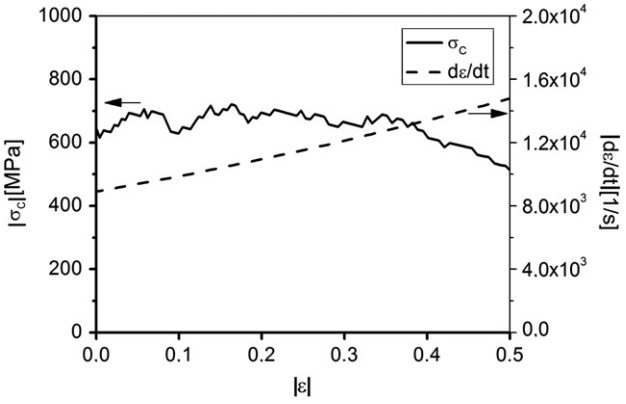

Fig. 3 – True stress and true strain rate as a function of true strain for the specimen tested at 29 m/s.

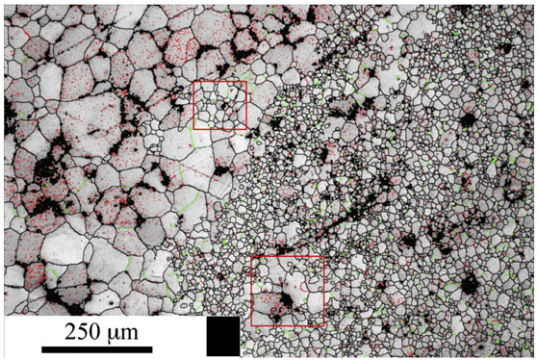

Fig. 4 – EBSD analysis of the impacted surface showing an inhomogeneous microstructure. The center of the sample (on the left side of the figure) consists mainly of coarse grains surrounded by a fine-grained rim (on the right side of the figure). The red and green lines correspond to LAGBs (see the text for more details).

consist of slipping, twinning, secondary twinning, kinking and cracking along grain boundaries and twin boundaries. Furthermore, the deformation and fracture mechanisms in polycrystalline Zn for different values of grain size and tensile strain rate were reported by Liu et al. [24]. It was shown that crack propagation was accompanied by formation of deformation twins and kinked bands, while in the vicinity of a grain boundary, cleavage crack first induced a plastic zone ahead, and then crossed the grain boundary when the strain accumulates. In the present case, when pure polycrystalline Zn was deformed at high strain rate, the microstructural observations do not show any evidence of twinning, contariwise to its appearance when the deformation was carried out in the quasi-static regime. Most probably, the lack of twins in the impacted sample is caused by the relatively small size of grains formed at high strain rate deformation as in *hcp* metals the reduction of grain size is usually accompanied by the decrease of twinning activity [25]. In smaller grains the stresses developed at dislocation pile-ups are higher that facilitate the operation of <c+a> dislocations beside <a> dislocations, thereby reducing the occurrence of twinning. Beside the small grain size, the higher deformation temperature also facilitates the activation of <c+a> dislocations, therefore in the case of Zn where RT corresponds to higher homologous temperature than for Mg or Ti, the critical grain size may be larger as smaller stresses are enough for the activation of <c+a> dislocations.

Further EBSD investigations of the impacted sample are shown in Fig. 5. Even if the information contained in the pole figures are incomplete and semi-quantitative, Fig. 5a indicates that in the coarse-grained central region the crystallographic orientation became more scattered after the impact test compared to the initial state (for instance, the basal poles tend to be tilted away from the normal of the impacted surface), while in the outer ring most of the fine grains have [0001] orientation parallel to the normal of the impacted surface, yielding an intense level of a [0001] fiber texture (see Fig. 5b). Former reports have shown that the combination of basal $\{0001\}<11\bar{2}0>$ slip and pyramidal $\{11\bar{2}2\}<11\bar{2}3>$ slip in Zn resulted in textures with basal poles tilted away from the normal direction toward the rolling direction [26]. In addition, in *hcp* metals reorientation of the grains due to recrystallization was also observed [27]. Therefore, both the dislocation activity during large impact deformation and the annealing processes, such as recovery and recrystallization usually occurring at high strain rates may result in the observed textural evolution. This is in line with TEM investigations as discussed below.

3.1.2. *TEM Investigations*

Fig. 6 shows qualitatively the typical microstructures observed by TEM after impact test. One quarter of the impacted disk was cut and within this piece three specimens were investigated, corresponding to the fine-grained outer ring (Fig. 6a), the intermediate zone (Fig. 6b) and the coarse-grained area in the center of the disk (Figs. 6c and d). Equiaxed and dislocation-free grains/crystallites are found within the fine-grained outer ring. It is noted that in the TEM micrographs some grains have much smaller size (about 500 nm) than the average value determined by EBSD (6 μm) that can be attributed to the step size used in EBSD investigations (about 1 μm). Moreover, differences between the grain size values observed by TEM and EBSD analyses are usually reported in the literature [28].

In the intermediate zone between the outer ring and the central area, another type of substructure is found which contains dislocation cells and a few isolated dislocations or dislocation debris (Fig. 6b). The observed substructure resembles to a polygonized structure similar to that develops during a recovery process. In the coarse-grained central area, the grains are populated with a high density of individual dislocations (see Fig. 6c) or dislocation networks (not shown). Both the TEM observation of the loose dislocation networks and the EBSD results indicating a large amount of LAGBs with small misorientations suggest a less correlated dislocation structure in the central coarse-grained region. Another characteristic feature of the microstructure is illustrated in

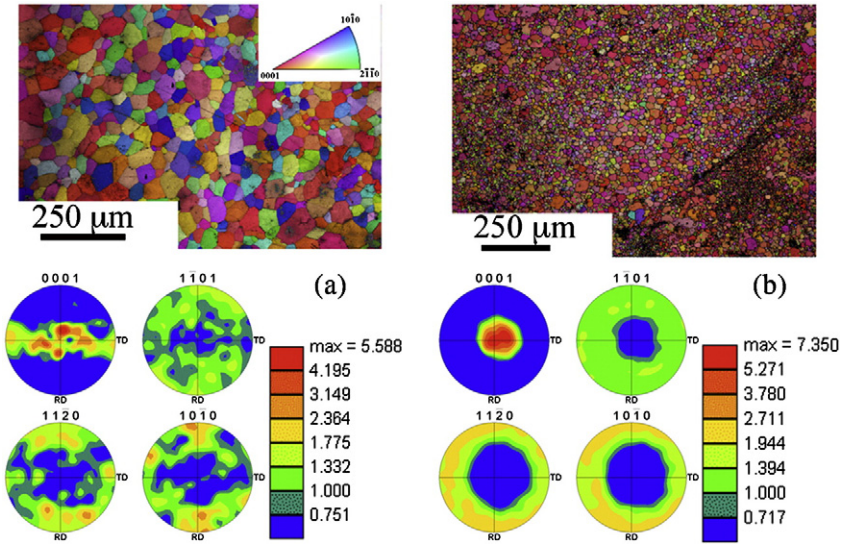

Fig. 5 – EBSD images showing the orientation distribution of the grains and the corresponding pole figures after the impact test for (a) the coarse-grained center and (b) the surrounding fine-grained zone.

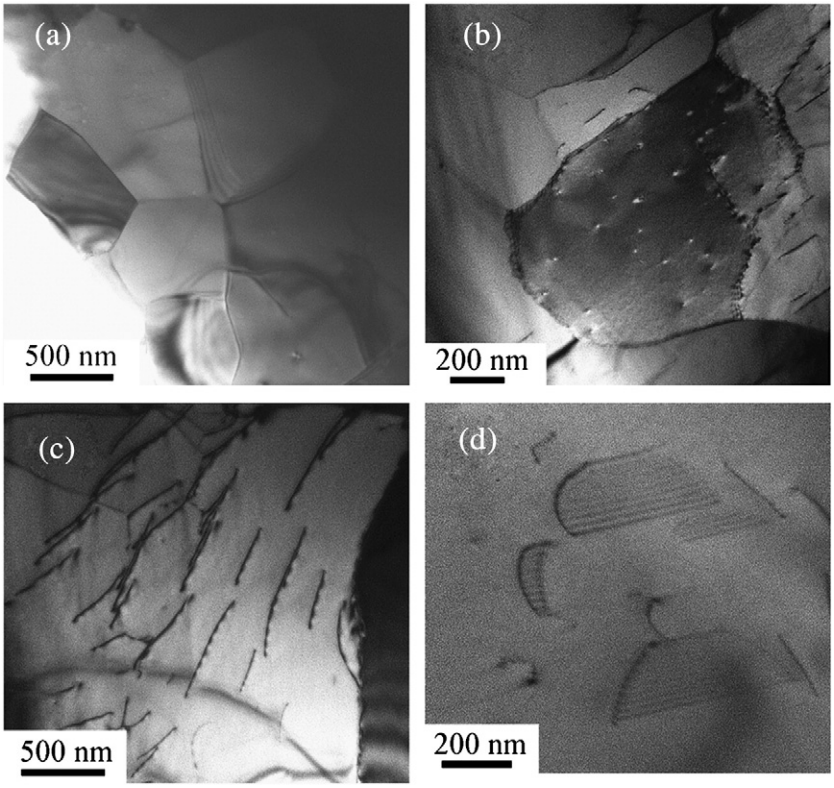

Fig. 6 – TEM images taken on different areas of the Zn sample impacted at a velocity of 29 m/s: outer ring having dislocation-free grains (a), the intermediate zone containing dislocation walls and some isolated dislocations (b), and the center part with large grains containing straight dislocation segments (c) as well as dislocation loops (d).

Fig. 6d which shows the presence of dislocation loops exhibiting fringes as they are inclined from the observation plane. This type of substructure was observed in both coarse-grained and fine-grained areas. Such loops were reported in high purity (99.999%) Zn quenched after annealing [29] and may have been formed by point defect agglomeration.

The dislocation-free grains and the polygonized dislocation structure suggest that recovery and/or recrystallization occurred due to the high strain and temperature rise in the short duration of the impact test. Local heating usually occurs due to the high strain rate impact as reported many times in the literature [9]. During high strain rate deformation, the fraction of plastic work, W_p that gets converted into heat in a unit volume during a supposedly adiabatic deformation process (assuming it is 90% of the plastic work) is related to the temperature increment as [30–32]:

$$\Delta T = \frac{0.9 W_p}{\rho C_p}, \tag{2}$$

where ρ is the mass density and C_p is the specific heat at constant pressure. The values of ρ and C_p for Zn are 7140 kg m^{-3} and 390 J kg^{-1} K^{-1}, respectively. Theoretically, this formula yields a temperature increment of $\Delta T \sim 660$ K. Therefore, during the high strain rate impact at RT the temperature of the sample may increase to $T + \Delta T \sim 960$ K, that is above the melting temperature of Zn (~692 K). This temperature level could have melted the specimen. Most probably, the surrounding material of the impact device dissipated a significant fraction of heat. In fact, the sample remained in contact with the impacting bar made of a tungsten alloy having very high thermal conductivity (~75 W/mK) that most probably led to a rapid cooling of the sample. Therefore, in such a case, the melting does not occur but the temperature remains high enough to trigger structural changes controlled, in part, by the strain gradient. The observed dislocation loops may be formed from point defects during cooling of the impacted sample. It is worth to note that Mishra et al. [33] have calculated the cooling rate in Cu sample severely deformed by a steel cylinder (thermal conductivity is ~35.17 W/mK) at RT and a strain rate of 1 s^{-1}. Their calculations showed that the sample cooled down from 355 K to RT within a time interval of 5 s.

As the center part contains significant amount of dislocations, while in the outer ring mostly defect-free grains are observed, most probably in the center there was only a recovery of the microstructure while in the ring recrystallization occurred during impact test. This inhomogeneity of the microstructure may be a consequence of both strain and temperature gradients. The recrystallization of the outer ring may be caused by the higher strain evolved there during deformation compared to the center region. This is caused by the bulging of the sample during impact test originating from the friction between the surfaces of the pressing bars and the sample. The higher strain in the outer ring yielded a higher driving force for recrystallization compared to the center part

where probably only recovery occurred. Such a strain gradient has been also reported in ECAP-processed Cu during high strain rate impact test [34].

As discussed in Section 3.1.1, the [0001] texture in the outer ring is most probably also formed due to recrystallization. The (0001) basal plane in Zn has the lowest surface energy [35] among the crystallographic planes, therefore this plane in the recrystallized grains is favourably lying parallel to the impacted surface. As a consequence, in both the annealed initial state and the recrystallized outer ring, [0001] texture was formed.

Finally, Schmid and Boas [36] have been also reported similar gradient in grain size for Sn sheets that were impacted by bullets at high strain rates. Around the holes left by the bullet impact, a recrystallized zone having fine grains was observed that was surrounded by a coarse-grained outer ring. The microstructure inhomogeneity was explained by the existence of a strain gradient, which was associated with the local increase of temperature resulting in dynamic recrystallization. It should be noted that the microstructure observed here is reversed to that discussed in [36]. In the present case, the average grain size in the center zone is much larger than in the outer ring. This apparent dichotomy can be explained by considering that in the case of a bullet impact the strain is the highest in the vicinity of the hole while in our case the strain is the largest at the periphery of the impacted disk.

3.2. *Nanoindentation Test*

Nanohardness measurements were carried out at five locations on the disk which are numbered from 1 to 5 as shown in Fig. 7a. The mean hardness was determined for each location from 400 indentations and plotted in Fig. 7b as a function of number of location. It can be revealed that the coarse-grained area possesses higher mean hardness value compared to the fine-grained outer ring. The observed mechanical behavior can be explained by the higher dislocation density in the center as follows.

Taking into account the strengthening caused by grain boundaries and dislocations using Hall–Petch and Taylor-formulas, respectively, the yield strength in the different areas of the impacted Zn sample can be approximated as:

$$\sigma = \sigma_0 + Kd^{-1/2} + \alpha MGb\rho^{1/2}, \quad (3)$$

where σ_0 is the friction stress, d is the grain size, α is a constant, M is the Taylor factor ($\alpha M \approx 1$), G is the shear modulus (40 GPa for Zn), b is the length of the Burgers vector (an average value of 0.42 nm was chosen assuming <a> and <c+a> dislocations with equal fractions) and ρ is the dislocation density. Using the values of $\sigma_0 = 23$ MPa and $K = 8.5$ MPa mm$^{1/2}$ taken from Ref. [37], as well as the grain size values determined by EBSD (20 and 6 μm for the coarse-grained center and the fine-grained outer ring, respectively), the contributions of grain boundaries to strength are 60 and 110 MPa for the coarse-grained center and the fine-grained outer ring, respectively. The average distance between dislocations estimated from Fig. 6c is 160 nm that corresponds to the dislocation density of 4×10^{13} m^{-2}. Substituting this value into Eq. (3), 105 MPa is obtained for the dislocation strengthening in the center region. As dislocation was only scarcely

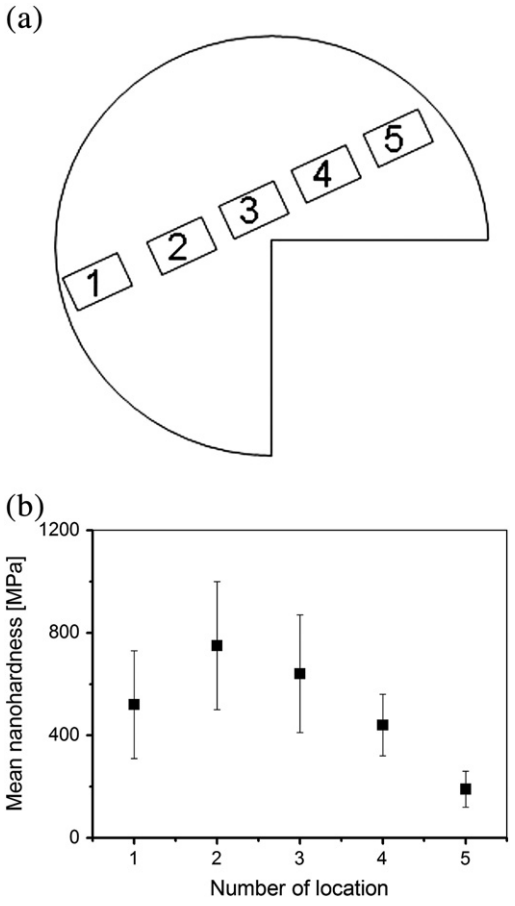

Fig. 7 – (a): The locations on the disk where nanohardness values were measured. The missing quarter was used for TEM investigations (see Section 3.1.2); (b): the mean nanohardness at different locations. Locations 2 and 3 correspond to the coarse-grained zone, while locations 1, 4 and 5 correspond to the surrounding fine-grained ring.

observed in the fine-grained outer ring, therefore in this region the dislocation strengthening was neglected. The calculation presented above shows that in the center zone the smaller grain boundary strengthening compared to the outer ring is overwhelmed by the dislocation strengthening, resulting in a higher total strength in the coarse-grained center than in the fine-grained outer ring. Assuming that the hardness is approximately three times of the yield strength, 600 and 400 MPa are obtained for the hardness of the center part and the outer ring, respectively, that are in good agreement with the experimental results (see Fig. 7b).

It should be noted that the [0001] texture in the outer ring may also affect the hardness value but it is difficult to estimate whether this texture increases or decreases the hardness compared to the case of random grain orientation as this effect depends on the type of active dislocation slip systems. As the Berkovich indenter used in this study is relatively flat, the resolved shear stresses in the planes lying perpendicular or parallel to the loading axis are low. Consequently, if [0001] texture exists, the basal and prismatic slips are difficult to occur under the tip, thereby increasing the hardness value compared to the case of random grain orientation. At the same

time, the slip on pyramidal planes are is easier for a *hcp* material having [0001] texture than for a randomly oriented grain structure. During plastic deformation of a *hcp* metal, usually basal and/or prismatic as well as pyramidal slips occur [38], therefore the [0001] texture may increase or decrease the hardness depending on the dislocation populations on the different slip planes.

4. Conclusions

High purity polycrystalline Zn was deformed at high strain rate by DIHPB. It was found that:

- The microstructure is considerably refined and an inhomogeneous grain structure developed, containing larger grains in the center region and finer grains in the rim. This microstructure is most probably caused by the strain gradient in the impacted sample. In the center part, where the strain is lower only recovery occurred while in the outer ring recrystallization took place due to the higher strain.
- Local mechanical measurements by nanoindentation showed that the large-grained area possesses higher hardness value compared to the fine-grained rim. This is attributed to the higher dislocation density in the center region whose hardening effect overwhelms the reduced strengthening due to the larger grain size compared to the outer ring.

Acknowledgments

This work was supported in part by the Hungarian Scientific Research Funds, OTKA, Grant No. K-81360. The European Union and the European Social Fund have provided financial support to this project under grant agreement no. TÁMOP 4.2.1./B-09/1/KMR-2010-0003.

REFERENCES

[1] Jenq ST, Chang H-H, Lai Y-S, Tsai T-Y. High strain rate compression behavior for Sn–37Pb eutectic alloy, lead-free Sn–1Ag–0.5Cu and Sn–3Ag–0.5Cu alloys. Microelectron Reliab 2009;49:310–7.
[2] Lee W-S, Liu C-Y, Sun T-N. Deformation behavior of Inconel 690 super alloy evaluated by impact test. J Mater Process Tech 2004;153–154:219–25.
[3] Chioua S-T, Cheng W-C, Lee W-S. Strain rate effects on the mechanical properties of a Fe–Mn–Al alloy under dynamic impact deformations. Mater Sci Eng A 2005;392:156–62.
[4] da Silva MG, Ramesh KT. The rate-dependent deformation and localization of fully dense and porous Ti–6Al–4 V. Mater Sci Eng A 1997;232:11–22.
[5] Gilat A, Cheng CS. Torsional split Hopkinson bar tests at strain rates above 10^4 s^{-1}. Exp Mech 2000;40:54–9.
[6] Regazzoni G, Kocks UF, Follansbee PS. Dislocation kinetics at high strain rates. Acta Metall 1987;35:2865–75.
[7] Zerilli FJ, Armstrong RW. The effect of dislocation drag on the stress–strain behaviour of F.C.C. metals. Acta Metall 1992;40:1803–8.
[8] Mishra A, Martin M, Thadhani NN, Kad BK, Kenik EA, Meyers MA. High-strain-rate response of ultra-fine-grained copper. Acta Mater 2008;56:2770–83.
[9] Dirras G, Couque H, Gubicza J, Ouarem A, Chauveau T, Jenei P. Fine-grained nickel deformed by direct impact at different velocities: microstructure and mechanical properties. Mater Sci Eng A 2010;527:4128–35.
[10] Ramesh KT. On the localization of shearing deformations in a tungsten heavy alloy. Mech Mater 1994;17:165–73.
[11] Odeshi AG, Al-ameeri S, Bassim MN. Effect of high strain rate on plastic deformation of a low alloy steel subjected to ballistic impact. J Mater Process Tech 2005;162–163:385–91.
[12] Wei Q, Schuster BE, Mathaudhu SN, Hartwig KT, Kecskes LJ, Dowding RJ, et al. Dynamic behaviors of body-centered cubic metals with ultrafine grained and nanocrystalline microstructures. Mater Sci Eng A 2008;493:58–64.
[13] Chichili R Deepak, Ramesh KT, Hemker KJ. Adiabatic shear localization in α-titanium: experiments, modeling and microstructural evolution. J Mech Phys Sol 2004;52:1889–909.
[14] Meyers MA, Subhash G, Kad BK, Prasad L. Evolution of microstructure and shear-band formation in α-hcp titanium. Mech Mater 1994;17:175–93.
[15] Lee W-S, Lin C-F, Liu T-J. Impact and fracture response of sintered 316 L stainless steel subjected to high strain rate loading. Mater Charact 2007;58:363–70.
[16] Xue Q, Liao XZ, Zhu YT, Gray III GT. Formation mechanisms of nanostructures in stainless steel during high-strain-rate severe plastic deformation. Mater Sci Eng A 2005;410–411:252–6.
[17] Hines JA, Vecchio KS. Recrystallization kinetics within adiabatic shear bands. Acta Mater 1997;45:635–49.
[18] Zhao WS, Tao NR, Guo JY, Lu QH, Lu K. High density nano-scale twins in Cu induced by dynamic plastic deformation. Scr Mater 2005;53:745–9.
[19] Zhang Y, Tao NR, Lu K. Mechanical properties and rolling behaviors of nano-grained copper with embedded nano-twin bundles. Acta Mater 2008;56:2429–40.
[20] Abdul-Latif A, Dirras GF, Ramtani S, Hocini A. A new concept for producing ultrafine-grained metallic structures via an intermediate strain rate: experiments and modeling. Int J Mech Sci 2009;51:797–806.
[21] Dirras G, Chauveau T, Abdul-Latif A, Ramtani S, Bui HQ. Microstructure characterization of high-purity aluminum processed by dynamic severe plastic deformation. Phys Stat Sol A 2010;207:2233–7.
[22] Couque H, Boulanger R. In: Gàlves F, Sanchez-Galves V, editors. Proceedings of the 23rd International symposium on Ballistics, Tarragona; 2007. p. 255–62.
[23] Li H, Duan QQ, Li XW, Zhang ZF. Compressive and fatigue damage behavior of commercially pure zinc. Mater Sci Eng A 2007;466:38–46.
[24] Liu JH, Huang CX, Wu SD, Zhang ZF. Tensile deformation and fracture behaviors of high purity polycrystalline zinc. Mater Sci Eng A 2008;490:117–25.
[25] Balogh L, Figueiredo RB, Ungár T, Langdon TG. The contributions of grain size, dislocation density and twinning to the strength of a magnesium alloy processed by ECAP. Mater Sci Eng A 2010;528:533–8.
[26] Wang YN, Huang JC. Texture analysis in hexagonal materials. Mater Chem Phys 2003;81:11–26.
[27] Hu H. Texture of Metals. Textures 1974;1:233–58.
[28] Bui QH, Dirras G, Ramtani S, Gubicza J. On the strengthening behavior of ultrafine-grained nickel processed from nanopowder. Mater Sci Eng A 2010;527:3227–35.
[29] Dobson PS, Smallman RE. The climb of dislocation loops in zinc. Proc Roy Soc A 1966;293:423–31.
[30] Mason JJ, Rosakis AJ, Ravichandran G. On the strain and strain rate dependence of the fraction of plastic work converted to heat: an experimental study using high speed

infrared detectors and the Kolsky bar. Mech Mater 1994;17: 135–45.
[31] Nemat-Nasser S, Ni L, Okinaka T. A constitutive model for fcc crystals with application to polycrystalline OFHC copper. Mech Mater 1998;30:325–41.
[32] Rittel D. On the conversion of plastic work to heat during high strain rate deformation of glassy polymer. Mech Mater 1999;31:131–9.
[33] Mishra A, Kad BK, Gregori F, Meyers MA. Microstructural evolution in copper subjected to severe plastic deformation: experiments and analysis. Acta Mater 2007;55:13–28.
[34] Lemiale V, Estrin Y, Seop Kim H, O'Donnell R. Grain refinement under high strain rate impact: a numerical approach. Comp Mater Sci 2010;48:124–32.
[35] Buckley DH. Surface effects in adhesion, friction, wear and lubrication, Tribilogy Series 5. Amsterdam: Elsevier; 1981.
[36] Schmid E, Boas W. Kristallplastizität. Berlin: Springer-Verlag; 1935.
[37] Chmelik F, Trojanova Z, Lukac P, Prevorovsky Z. Acoustic emission from zinc deformed at room temperature Part II The influence of grain size on deformation behaviour and acoustic emission of pure zinc. J Mater Sci Lett 1993;12:1166–8.
[38] Ungár T, Gubicza J. Nanocrystalline materials studied by powder diffraction line profile analysis. Z Kristallogr 2007;222:114–28.